JOURNAL OF COMPUTATIONAL PHYSICS 84, 326–342 (1989)

# A Comparison of Numerical Methods for Solving Nonlinear Integral Equations Found in Liquid Theories

LUIS MIER Y TERÁN, ENRIQUE DÍAZ-HERRERA, AND MARCELO LOZADA-CASSOU

*Departamento de Física,*
*Universidad Autónoma Metropolitana-Iztapalapa,*
*Apartado Postal 55-534, 09340 D.F., México*

AND

RAFAÉL SAAVEDRA-BARRERA

*Departamento de Ingeniería Eléctrica,*
*Universidad Autónoma Metropolitana-Iztapalapa,*
*Apartado Postal 55-534, 09340 D.F., México*

Received June 21, 1988; revised November 28, 1988

The accuracy and efficiency of several numerical methods for solving nonlinear integral equations typically found in liquid state theories is studied. In particular, we solve the so-called hypernetted chain-mean spherical approximation (HNC/MSA) system of integral equations. These equations are solved through the succesive substitution method and collocation and Galerkin's versions of the finite element method. It is found that finite element functional analysis, combined with Newton's method, produces especially accurate and efficient algorithms. © 1989 Academic Press, Inc.

## 1. INTRODUCTION

The structure of a simple fluid in equilibrium is defined in terms of probability densities for finding two, three, or more particles at specified locations in space. Many of the theories for the distribution functions of both homogeneous or inhomogeneous fluids are formulated in terms of nonlinear integral or integro-differential equations [1]. Although there are a few very important cases for which some of these theories can be analytically solved [1], their application to many other situations of physical relevance inevitably requires numerical iterative methods [2]. Among the most extensively used numerical procedures are the successive substitution method or Picard iterative method [2–5] and the Fourier



0021-9991/89 $3.00

transform method [2, 6]. In many cases the results obtained with those procedures are satisfactory but, too often, the sensitivity to the choice of a trial function leads to difficulties in getting the iterative scheme to converge [4, 7]. When these difficulties are present, if success is awaiting, solving nonlinear equations requires numerous iterations and thus large amounts of computational time. This situation can even be harder when ionic fluids are involved [8].

In the past, an efficient numerical algorithm based on the finite element method was applied to the solution of the Percus–Yevick (PY) and hypernetted chain (HNC) integral equations, for a fluid of particles interacting through a 6–12 Lennard–Jones pair potential [9], and to the mean spherical approximation (MSA), for the square-well [10, 11] and Yukawa fluids [12, 13]. Other efficient numerical methods, based on the Newton–Raphson iterative technique, have been developed [14, 15].

In this article, we compare the efficiency and accuracy of a successive substitution method against three different versions of the finite element technique, when solving the HNC/MSA coupled nonlinear integral equations for a model electrolyte solution next to a charged electrode. In this model, which is known as the primitive model, the ions of species $i$ are charged hard spheres of charge $z_i e$ and diameter $a_i$, the solvent is a dielectric continuum of dielectric constant $\varepsilon$, and the electrode is taken to be a flat, hard wall with a charge density $\sigma$. We believe that this comparison can be of help for a more appropriate choice of numerical algorithm when solving systems of nonlinear integral equations similar to the HNC/MSA solved here.

In the next section we describe some details of the theory associated with the HNC/MSA integral equation. Section 3 is devoted to a discussion of the numerical methods used in this work. We use Section 4 to make some comparisons of the accuracy and efficiency of the four numerical methods. The accuracy is tested through the charge density $\sigma$ on the surface of the electrode, a quantity that, as we shall see, can be calculated from the solution functions of the integral equations. The efficiency is tested through the computing time required by the four procedures. In Section 5 we present some conclusions about the accuracy that each of the methods can offer and their computing time consumption.

## 2. Theory

In the primitive model of an electrolyte the interaction potential between two ions separated a distance $r$ is

$$U_{ij}(r) = \begin{cases} \infty, & r < a_{ij} \\ \dfrac{z_i z_j e^2}{\varepsilon r}, & r > a_{ij}. \end{cases} \tag{1}$$

Where $z_i$ is the valence (including sign) of ion of species $i$, $e$ is the magnitude of the electronic charge, and

$$a_{ij} = \frac{a_i + a_j}{2}.$$

If a charged wall or electrode is immersed into an electrolyte, ions of opposite charge accumulate near the wall. The charged electrode and the accumulation of charge form a "double layer" of charge. Therefore one refers to this system as the electrical double layer system. For simplicity we assume that all the ions are equal in diameter. Consequently all the ions have the same distance of closest approach, $a/2$, to the plane, where $a$ is the ionic diameter common to all the species. For a discussion on this and other models of the electrical double layer see Ref. [16].

The interaction potential between an ion with the electrode is given by

$$U_i(x) = \begin{cases} \infty, & x < a/2 \\ -\dfrac{4\pi e z_i \sigma}{\varepsilon} x + c, & x \geqslant a/2. \end{cases}$$

where $x$ is the ion's distance to the plate and $c$ is a constant which depends on the choice of the point of zero potential. A singlet distribution function, $g_i(x)$, of ions of species $i$ at a distance $x$ from the wall is defined as

$$g_i(x) = \frac{\rho_i(x)}{\rho_i},$$

where $\rho_i(x)$ is the species $i$ number density profile and $\rho_i = \rho_i(\infty)$ is its bulk number density. The function $g_i(x)$ is a measure of the probability of finding an ion of species $i$ at a distance $x$ from the plate. Therefore in our model $g_i(x) = 0$ for $x < a/2$.

The mean electrostatic potential at a distance $x$ from the wall is given by [4]

$$\psi(x) = \frac{4\pi e}{\varepsilon} \sum_{j=1}^{n} z_i \rho_i \int_x^\infty (x - t)\, g_i(t)\, dt, \tag{2}$$

where $n$ is the number of species in the electrolyte.

The charge density $\sigma$ on the electrode must be equal in magnitude, but opposite in sign, to the total amount of charge accumulated near the electrode. Hence

$$\sigma = -e \sum_{i=1}^{n} z_i \rho_i \int_0^\infty g_i(t)\, dt. \tag{3}$$

The HNC/MSA integral equations for the reduced density profiles, $g_i(x) = h_i(x) + 1$, are [4]

$$1 + h_i(x) - \exp\left\{ -ez_i\beta\psi_0 + 2\pi\rho A(x) + 2\pi \sum_{j=1}^{n} \rho_j \int_{a/2}^{\infty} h_j(t)\, K(x, t)\, dt \right.$$
$$\left. + \frac{2\pi\beta e^2 z_i}{\varepsilon} \sum_{j=1}^{n} z_j \rho_j \int_{a/2}^{\infty} h_j(t)\, L(x, t)\, dt \right\} = 0 \tag{4}$$

for $i = 1, ..., n$, where $\beta = 1/kT$ ($k$ is Boltzmann's constant and $T$ is absolute temperature); $\psi_0$ is the electrostatic potential on the plate,

$$A(x) = -\left(\frac{c_1}{2} + \frac{c_2}{3} - \frac{c_3}{5}\right)\left(\frac{3a}{2} - x\right) a^2$$
$$- \frac{c_1}{6}\left[\left(x - \frac{a}{2}\right)^3 - a^3\right] - \frac{c_2}{12a}\left[\left(x - \frac{a}{2}\right)^4 - a^4\right]$$
$$+ \frac{c_3}{30a^3}\left[\left(x - \frac{a}{2}\right)^6 - a^6\right], \qquad x < \frac{3a}{2}$$
$$= 0, \qquad x > \frac{3a}{2}; \tag{5}$$

$$K(x, t) = \frac{c_1}{2}\left[a^2 - |x - t|^2\right] + \frac{c_2}{3a}\left[a^3 - |x - t|^3\right]$$
$$- \frac{c_3}{5a^3}\left[a^5 - |x - t|^5\right], \qquad x - a < t < x + a$$
$$= 0, \qquad \text{otherwise}; \tag{6}$$

$$L(x, t) = -2t, \qquad t < x - a$$
$$= a - x - t - \frac{\Gamma}{1 + \Gamma a}\left[a^2 - (x - t)^2\right]$$
$$+ \frac{1}{3}\left(\frac{\Gamma}{1 + \Gamma a}\right)^2 (a^3 - |x - t|^3), \qquad x - a < t < x + a$$
$$= -2x, \qquad x + a < t. \tag{7}$$

In Eqs. (5) and (6),

$$c_1 = -\frac{(1 + 2\eta)^2}{(1 - \eta)^4}, \tag{8}$$

$$c_2 = 6\eta \frac{(1 + \eta/2)^2}{(1 - \eta)^4}, \tag{9}$$

$$c_3 = -\eta \frac{c_1}{2}, \tag{10}$$

$$\eta = \pi\rho a^3/6, \tag{11}$$

$$\rho = \sum_{i=1}^{n} \rho_i,$$

$$\Gamma = \frac{(1+2\kappa a)^{1/2} - 1}{2a}, \tag{12}$$

and

$$\kappa^2 = \frac{4\pi\beta e^2}{\varepsilon} \sum_{i=1}^{n} z_i^2 \rho_i \tag{13}$$

is the Debye screening length; $\kappa^{-1}$ is a measure of the thickness of the electrical double layer. The higher the concentration and/or the valence of the ions the smaller the thickness of the double layer.

The HNC/MSA equations have been previously solved for some two species symmetric ($z_1 = -z_2$) [4] and asymmetric salts [5]. In all cases the ionic concentrations $\rho_1$ and $\rho_2$ were chosen in order to satisfy the charge neutrality condition

$$\sum_{i=1}^{n} z_i \rho_i = 0, \tag{14}$$

since this condition, although not neccessary, has been imposed in the derivation of Eqs. (4).

The agreement of the HNC/MSA calculations with Monte Carlo results, which are the "experimental" results for the given model, shows the Eqs. (4) satisfactorily account for the interfacial properties of the primitive model of an electrolytic solution near a flat electrode [4, 5].

## 3. Numerical Methods

A common feature of numerical algorithms for solving nonlinear integral equations is the transformation of the problem into a set of nonlinear algebraic equations. In most numerical approximation processes, a trial function is expressed in terms of a set of basis functions, and the coefficients of the basis functions in the expression are related by executing some scheme for reducing a measure of the error of approximation. In some cases the unknowns of the algebraic system agree, up to some approximation, with the values of the unknown solutions of the integral equation at certain properly selected points of the domain. A wide variety of basis functions have been used to obtain solutions of the integral equations of statistical

mechanics. For example, Lozada *et al.* [4, 5] employed quadratic functions when they evaluated the integrals of Eqs. (4) by Simpson's rule while Alvarez *et al.* [17] constructed an appropriate set of domain-spanning orthogonal polynomials to solve the same equations. Different algorithms produce different sets of algebraic equations which must be solved by iteration in order to complete the solution of the integral equation. In this section we outline the procedures used in this work for solving HNC/MSA integral equations for the electrical double layer. These are, the successive substitution method, the collocation version of the finite element method both with linear and quadratic basis functions and the Galerkin's versions of the finite element method with linear basis functions.

*Successive Substitution Method*

The form of Eqs. (4) is well suited for the use of the successive substitution method. The successive substitution method employed in this work was used before by Lozada *et al.* [4, 5] to solve the same set of equations. In this method, the set of integral equations is transformed into a set of algebraic equations by substitution of the integrations in (4) by a quadrature rule. Following Ref. [4] we used Simpson's rule in this work. Since solving an equation on an unbounded domain is clearly impractical, it is assumed that the reduced density profiles, $g_i(x)$, are equal to unity for $x$ greater than a cutoff value, $R$. The value of $R$ is strongly dependent on the concentration of the electrolyte, being necessary to choose it by successive increments in its value until the solution is stable.

In order to solve the system (4) for given values of $\beta$, $\psi_0$ and concentration, some initial set of guess functions, $h_{\text{in};i}(x)$, is inserted into the right-hand side of Eqs. (4) to obtain a first-improved guess $h_{\text{out};i}(x)$. In principle these functions could be reinserted into the right-hand side of the equations and a second improved set of function obtained. Iteration in this manner could produce a series of approximations convergent to the correct solution. However, generally this results in an extremely lengthy and frequently unstable procedure. Fortunately, the iteration convergence can be improved by mixing successive values of $h_i(x)$, according to the formula

$$h_{\text{in};i}^{(s+1)}(x) = \lambda h_{\text{out};i}^{(s)}(x) + (1-\lambda)\, h_{\text{in};i}^{(s)}(x), \tag{15}$$

where $\lambda$ is a parameter that must be decreased with increasing concentration. The iterative process is continued until some measure of the difference between succesive iterations become less than a prescribed small number $\Delta$. In this work we used the Euclidean norm as that measure; that is,

$$\left[\sum_{i=1}^{n}\sum_{j=1}^{n}(h_{\text{out};i}(x_j) - h_{\text{in};i}(x_j))^2\right]^{1/2} \leqslant \Delta, \tag{16}$$

where $n$ is the number of species in the electrolyte and $N$ is the number of points used in the numerical integration.

*Finite Element Methods*

The goal of the finite element method is to reduce a set of equations $\mathscr{L}[\mathbf{h}(x)] = 0$ to a system of algebraic equations by subdividing the domain of the problem into a number of subdomains, or elements, of appropriate size and shape. The solution functions, $h_i(x)$, in Eqs. (4) are approximated by a set of $N$ linearly independent basis functions $\{\phi_i(x)\}$,

$$h_i^a(x) = \sum_{k=1}^{N} h_{ij}\phi_j(x). \tag{17}$$

In the last equation, the superscript $a$ emphasizes the approximate character of the function $h_i(x)$. The functions $\phi_j(x)$ have simple mathematical forms and are defined piecewise over the finite element mesh. The unknown coefficients, $\{h_{ij}\}$, are approximations for the values of the solution function $h_i(x)$ evaluated at the nodes of the elements.

When the expansion (17) is substituted into Eqs. (4), the discrepancies between the actual and approximate solutions, i.e., the residual functions, $\mathscr{L}[\mathbf{h}^a]$, are obtained:

$$\mathscr{L}_i[\mathbf{h}^a(x)] = 1 + \sum_{k}^{N} h_{ik}\phi_k(x) - \exp\left\{-ez_i\beta\psi_0 + 2\pi\rho A(x) + 2\pi\sum_{j}^{n}\sum_{k}^{N}\rho_j h_{jk}K_k(x) + \frac{2\pi\beta e^2 z_i}{\varepsilon}\sum_{j}^{n}\sum_{k}^{N} z_j\rho_j h_{jk}L_k(x)\right\}, \tag{18}$$

for $i = 1, ..., n$. Where the functions $K_k(x)$ and $L_k(x)$ are defined as

$$K_k(x) \equiv \int_{a/2}^{R} K(x, t)\,\phi_k(t)\,dt, \tag{19a}$$

and

$$L_k(x) \equiv \int_{a/2}^{R} L(x, t)\,\phi_k(t)\,dt. \tag{19b}$$

The weighted-residuals method provides criteria for minimizing the residual functions, $\mathscr{L}[\mathbf{h}^a(x)]$. In the collocation [18] version of this method the residuals are reduced to zero at the nodes of the elements,

$$\int_{a/2}^{R} \mathscr{L}[\mathbf{h}^a(x)]\,\delta(x - x_l)\,dx = 0 \tag{20}$$

for $l = 1, ..., N$, where $\delta(x - x_l)$ is the Dirac delta function and $x_l$ is the value of $x$ at the $l$th node. This is a discrete form of the variational problem in which Eqs. (4) are asked to hold in the most classical sense. On the other hand, in its most obvious

form, Galerkin's method [18] requires the residual functions to be orthogonal with all the approximating functions $\phi_l(x)$,

$$\int_{a/2}^{R} \mathscr{L}[\mathbf{h}^a(x)]\, \phi_l(x)\, dx = 0, \tag{21}$$

for $l = 1, ..., N$. Galerkin's method is a weak or non-classical formulation of the variational problem.

Substituting Eqs. (18) into the collocation criteria, Eqs. (20), we obtain the system of algebraic equations,

$$F_{il} = 1 + h_{il} - E_i(x_l) = 0 \tag{22}$$

for $i = 1, ..., n$ and $l = 1, ..., N$. The function $E_i(x; \mathbf{h})$ is defined by

$$E_i(x) \equiv \exp\left\{ -ez_i\beta\psi_0 + 2\pi\rho A(x) + 2\pi \sum_j^n \sum_k^N \rho_j h_{jk} K_k(x) + \frac{2\pi\beta e^2 z_i}{\varepsilon} \sum_j^n \sum_k^N z_j \rho_j h_{jk} L_k(x) \right\}. \tag{23}$$

On the other hand, substitution of Eqs. (18) into the Galerkin's criteria, Eq. (21), yields the set of algebraic equations,

$$\sum_k h_{ik} a_{kl} - f_{il}(\{h\}) + b_l = 0 \tag{24}$$

for $i = 1, ..., n$ and $l = 1, ..., N$, where

$$a_{kl} \equiv \int_{a/2}^{R} \phi_k(x)\, \phi_l(x)\, dx, \tag{25}$$

$$f_{il}(\{h\}) \equiv \int_{a/2}^{R} \phi_l(x)\, E_i(x; \{h\})\, dx, \tag{26}$$

and

$$b_l \equiv \int_{a/2}^{R} \phi_l(x)\, dx. \tag{27}$$

The matrix elements $a_{kl}$ and the vector elements $b_l$, which involve only integrals of the basis functions, can be computed once and for all. Numerical calculation of $f_{il}$ could require numerous evaluations of the function $E_i(x)$. The next numerical approximation we make is to expand the function $E_i(x)$ in the basis functions $\{\phi_i(x)\}$; that is,

$$E_i(x) = \sum_k^N e_{ik} \phi_k(x). \tag{28}$$

This is called the Swartz–Wendroff approximation [19]. When this approximation is used, the integrals in (26) can be expessed as

$$f_{il} = \sum_{k}^{N} e_{ik} a_{kl}. \tag{29}$$

The coefficients $e_{ik}$ are the values of the function $E_i(x)$ at the nodes; that is, $e_{ik} = E_i(x_k)$.

Expressions (28) allows us finally to write the Galerkin equations, Eqs. (24), in the simple form,

$$F_{il} = \sum_{k}^{N} (h_{ik} - e_{ik})\, a_{kl} + b_l = 0 \tag{30}$$

for $i = 1, ..., n$ and $l = 1, ..., N$. In contrast with Eqs. (24), this new set of algebraic equations only requires evaluation of the functions $E_i(x)$ at the nodes of the elements.

The key feature of the finite-element approach is that each basis function is non-zero only over a small subdomain of the entire domain $a/2 < x < R$. In this work we used two different sets of basis functions: linear and quadratic Lagrange shape functions. First we define a local variable $\xi$ taken values in the interval, $-1 \leqslant \xi \leqslant 1$, over each finite element,

$$\xi = \frac{2x - x_l - x_r}{x_r - x_l}, \tag{31}$$

where $x_1$ and $x_r$ are the positions of the left and right endpoints of the element, respectively. Two local linear functions are then defined over each element

$$\phi_1^e(\xi) = \tfrac{1}{2}(\xi + 1) \tag{31a}$$

and

$$\phi_2^e(\xi) = \tfrac{1}{2}(1 - \xi). \tag{31b}$$

Similarly, three local quadratic functions are defined over each element

$$\phi_1^e(\xi) = \tfrac{1}{2}\xi(\xi - 1), \tag{32a}$$

$$\phi_2^e(\xi) = 1 - \xi^2, \tag{32b}$$

and

$$\phi_3^e(\xi) = \tfrac{1}{2}\xi(\xi + 1). \tag{32c}$$

Quadratic functions require an auxiliary node at the middle point of the element.

Once a set of basis functions is selected, equations for the collocation or Galerkin criteria can be solved by Newton's method. This algorithm provides a set of linear equations for the expansion coefficients at the $(k+1)$-th iteration in terms of the coefficients at the $k$th iteration. In compact notation

$$\mathbf{J}(\mathbf{h}^{(k)}) \cdot (\mathbf{h}^{(k+1)} - \mathbf{h}^{(k)}) = -\mathbf{F}(\mathbf{h}^{(k)}), \tag{33}$$

where $\mathbf{J}$ is the Jacobian matrix of the system.

Gaussian elimination was used to solve Eq. (33). The iterative process is continued until the Euclidean norm of the difference between succesive iterations become less than a prescribed small number $\Delta$:

$$\|\mathbf{h}^{(k+1)} - \mathbf{h}^{(k)}\| = \left[ \sum_{i=1}^{n} \sum_{j=1}^{N} (\mathbf{h}_{ij}^{(k+1)} - \mathbf{h}_{ij}^{(k)})^2 \right]^{1/2} \leqslant \Delta. \tag{34}$$

This is equivalent to the criteria used to stop the successive substitution process, Eq. (16).

The converged Jacobian from Newton's method was used to provide initial estimates of solutions for other conditions by a first-order parametric continuation technique, similar to Euler's method. If, for example, the potential $\psi_0$ on the electrode is chosen as the changing parameter, an initial estimate $\mathbf{h}'$ for a larger potential $\psi_0'$ can be generated from the converged Jacobian of a previous solution $\mathbf{h}$ at a lower value $\psi_0$ by

$$\mathbf{J}(\mathbf{h}; \psi_0) \cdot (\mathbf{h}' - \mathbf{h}) = -\left(\frac{\partial \mathbf{F}}{\partial \psi_0}\right)_{\psi_0} (\psi_0' - \psi_0). \tag{35}$$

## 4. Results

Having established the equations for the collocation and Galerkin methods, in this section we proceed to do some comparisons between the results obtained with these methods and the successive substitution method. We solved Eqs. (22) for the collocation criteria using both linear and quadratic basis functions, Eqs. (31) and (32), respectively. We also solved Eqs. (29) for the Galerkin criteria with the Swartz–Wendroff approximation using linear basis functions. In order to solve those equations, the domain $a/2 \leqslant x \leqslant R$ was divided into suitable finite elements. The positions of the nodes, $\{x_i\}$, were chosen to concentrate elements in those portions of the domain where the solution varies most rapidly. Because reduced density profiles are very steep near the hard wall, this option is particularly important for the integral equation under study. In this work, the domain was divided into several subdomains, and a uniform grid was constructed over each one of them. To illustrate the general form of the solution, in Fig. 1 we show the reduced density profiles for a typical example. It is seen in this figure that the counterion reduced

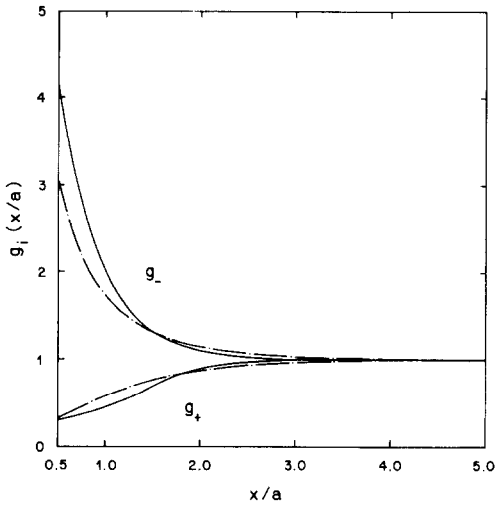


FIG. 1. Reduced density profiles for a 1 M model monovalent electrolyte ($a = 4.25$ Å, $T = 298$ K, $\varepsilon = 78.5$). The potential on the electrode is $\psi_0 = 50$ mV. The broken and solid curves correspond to Gouy–Chapman and HNC/MSA results, respectively.

density, $g_-(x)$, is, of course, higher next to the positively charged electrode and decreases as $x$ increases, since the electric field produced by the electrode is gradually being screened by the counterions charge. Whereas the co-ion reduced density has the opposite behavior. The distance from the plate to the point where the co-ion and counterion become equal to their bulk value ($g_i(x) = 1$) is called the thickness of the electrical double layer. The higher the ionic concentration and/or valence and/or the potential of the plate, the smaller the thickness of the electrical double layer. For comparison, in the same figure the results obtained with the classical theory of Gouy [20] and Chapman [21] are also shown. In the version Gouy and Chapman used here, the ions are assumed to be point charges. However, they are assumed to have a size in their interaction with the plate. Therefore this theory mainly takes into account the effect of the electrical forces present in the system. Whereas the HNC/MSA result in addition takes into account in an approximate manner the ionic size. It is seen in Fig. 1, that there are quantitative and qualitative differences between the two theories. For example, notice that the thickness of the electrical double layer is narrower in the HNC/MSA result.

In order to study how the accuracy of the solution improves when the number of elements on the domain is increased, we choose first to solve the case of a symmetrical 1: 1 electrolyte with a concentration of 1 M, and electrode potential of $\psi_0 = 10$ mV. All calculations were done with $a = 4.25$ Å, $\varepsilon = 78.5$, and $T = 298$ K. For this concentration, an appropriate value of the cutoff is $R = 20$ (distances are reduced with the distance of closest approach, a/2). Eight different grids were used in this case. In Table I the number of elements (two node elements) over each one of four subdomains is tabulated. Hereafter we refer to these grids as G1 to G8.

TABLE I

Finite Element Grids

| Interval $\frac{x}{a/2}$ | Grids | | | | | | | |
|---|---|---|---|---|---|---|---|---|
| | G1 | G2 | G3 | G4 | G5 | G6 | G7 | G8 |
| 1–3 | 10 | 20 | 20 | 30 | 40 | 40 | 80 | 160 |
| 3–6 | 9 | 9 | 18 | 18 | 18 | 30 | 60 | 120 |
| 6–12 | 9 | 9 | 18 | 18 | 18 | 24 | 24 | 24 |
| 12–20 | 4 | 4 | 4 | 4 | 4 | 4 | 4 | 4 |
| Total | 32 | 42 | 60 | 70 | 80 | 98 | 168 | 308 |

*Note.* The domain $1 \leqslant x \leqslant 20$, was divided into four subdomains and a uniform mesh formed over each one. First column on the left shows the limits of each subdomain and other columns show the number of two nodes elements on the subdomain. Distances are expressed in units of $a/2$.

Starting from the Gouy–Chapman approximation, which can be solved analytically, as trial functions, we obtained solutions of the HNC/MSA approximation with the four options described at the beginning of this section. The iterative processes are deemed to have converged for $\Delta = 10^{-10}$ (see Eq. (16) for Picard iteration and Eq. (34) for Newton's iteration).

To measure the accuracy of the four numerical methods one could calculate from the solution of the HNC/MSA equations the electrostatic potential on the plate, which from Eq. (2) is equal to

$$\psi_0 \equiv \psi(0) = -\frac{4\pi e}{\varepsilon} \sum_{j=1}^{n} z_j \rho_j \int_0^\infty t g_j(t)\, dt.$$

This quantity should give us the input value of $\psi_0$. Unfortunately, while the collocation and Galerkin methods with linear basis functions recover the value of $\psi_0$ poorly and are very sensitive to the grid, the quadratic basis versions of the collocation and the Picard methods recover the value of $\psi_0$ outstandingly and almost independently of the grid chosen.

To facilitate comparisons, we performed calculations of the charge density on the plane, $\sigma$, according to Eq. (3). This quantity is much more sensitive to the grid chosen. In Table II we present the results obtained with each of four options for grids G1 to G8. As was expected, the four options compared tend to a certain limit value of the charge density, $\sigma_0$, as the number of elements is increased. While the two options that employ linear basis functions (options 2 and 4) result in very similar values of $\sigma$, when the same grid is used, options that employ quadratic basis functions (options 1 and 3), do not in general agree in the value of $\sigma$ when they have the same grid. However, they seem to tend to the limit of $\sigma_0$ quicker than the linear basis function methods. Therefore, options 1 and 3 are probably more

TABLE II

Charge Density $\sigma$ on the Electrode for a 1 M Monovalet Electrolyte in c/m$^2$

| Option | G1 | G2 | G3 | G4 | G5 | G6 | G7 | G8 |
|---|---|---|---|---|---|---|---|---|
| 1 Picard | 1.6228835 | 1.6228417 | 1.6227726 | 1.6227732 | 1.6227643 | 1.6227660 | 1.6227661 | 1.6227661 |
| 2 Collocation linear basis | 1.6162159 | 1.6171512 | 1.6211210 | 1.6212940 | 1.6213545 | 1.6224426 | 1.6226567 | 1.6227103 |
| 3 Collocation quadratic basis | 1.6227959 | 1.6227925 | 1.6227683 | 1.6227681 | 1.6227679 | 1.6227664 | 1.6227664 | 1.6227664 |
| 4 Galerkin linear basis | 1.6162145 | 1.6171479 | 1.6211195 | 1.6212925 | 1.6213530 | 1.6224411 | 1.6226552 | 1.6227087 |

*Note.* $a = 4.24$ Å, $z = 1$, $T = 298$ K, $\varepsilon = 78.5$. The electrode has a potential, $\psi_0 = 10$ mV. This quantity was calcultated using the four options described in the first column on the left for each of the grids in Table I.

accurate than the other two. Hence we have arbitrarily determined the value of $\sigma_0$ as the mean value of $\sigma$ for options 1 and 3 with G8. Thus $\sigma_0 = 1.62276624 \pm 1.2 \times 10^{-7}$.

In Fig. 2 we plot a measure of the relative deviation from $\sigma_0$, for each of the four options, against the number of elements. Since the grids used are uneven, the scale in the abscissa is somewhat artificial. Nevertheless, the figure shows how the relative deviation decreases as $N$ increases. Options 1 and 3 are clearly better than options 2 and 4. Option 3 seems to tend to the $\sigma_0$ limit in a more consistent way than option 1. Options 2 and 4 would require an impractical number of elements to attain values of the order of $10^{-7}$ or less.

The efficiency of the methods is measured in terms of the computing time needed to obtain solutions of the HNC/MSA integral equations. Our values of computing time for each of the four options for grids G1 to G8 are given in Table III. For comparison, we arbitrarily assigned a value of unity to the computing time of option 3 with G6. In a CDC-930 this corresponds to a CPU time of 3.27 min. It is apparent from this table that Picard iteration, option 1, is extremely expensive compared with the other options for the grid used in this work. However, it is also apparent that the rate at which computing time increases is lower for Picard iteration than for any of the options considered. As was expected, Galerkin's

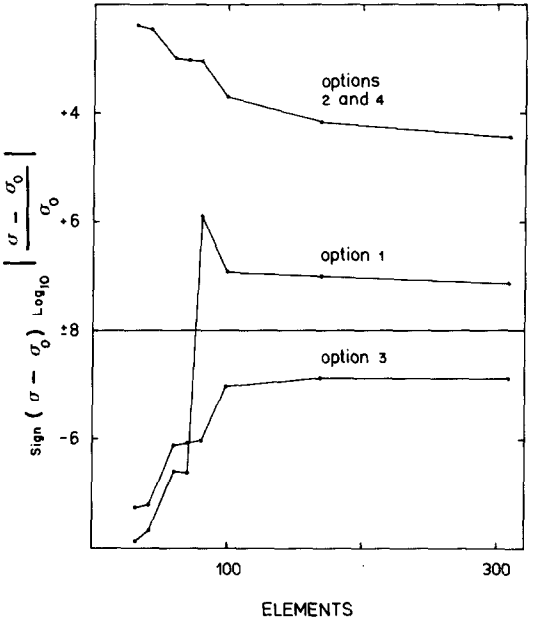


FIG. 2. Relative deviation of the charge density, $\sigma$, against the total number of elements. Since the values of $\sigma$ obtained with a given number of elements are dependent on the positions of the nodes, $\{x_i\}$, the scale for the abscissa is somewhat artificial. These results correspond to a symmetrical 1:1 electrolyte with a concentration of 1 M and $\psi_0 = 10$ mV ($a = 4.25$ Å, $T = 298$ K, $\varepsilon = 78.5$).

TABLE III

Computing Time Consumption for Each of the Four Options

| | Grids | | | | | | | |
|---|---|---|---|---|---|---|---|---|
| Option | G1 | G2 | G3 | G4 | G5 | G6 | G7 | G8 |
| 1 | 2.10 | 3.52 | 4.33 | 8.41 | 8.96 | 11.13 | 31.2 | 100.90 |
| 2 | 0.05 | 0.10 | 0.25 | 0.49 | 0.70 | 0.99 | 4.65 | 27.20 |
| 3 | 0.07 | 0.15 | 0.26 | 0.49 | 0.57 | 1.00 | 4.64 | 27.20 |
| 4 | 0.08 | 0.15 | 0.45 | 0.54 | 0.96 | 1.69 | 10.00 | 44.20 |

*Note.* A unit time was arbitrarily assigned to option 4 with grid G6.

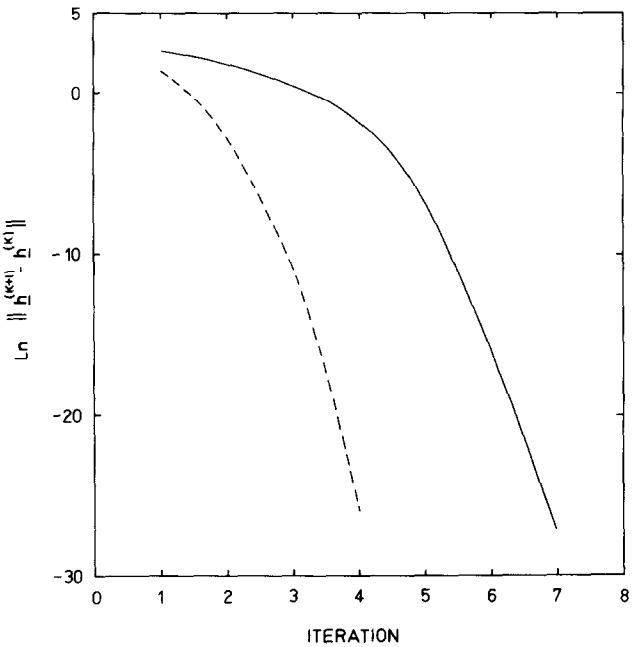


FIG. 3. Typical convergence of the solutions of HNC/MSA equations for a 1 M model monovalent electrolyte ($a = 4.25$ Å, $T = 298$ K, $\varepsilon = 78.5$). The logarithm of the Euclidean norm as a function of the number of iterations, when $\psi_0 = 50$ mV, is shown. The upper curve corresponds to Newton's iterative process when the initial guess function is the solution of the HNC/MSA equation for the $\psi_0 = 10$ mV case. The lower curve (broken) corresponds to Newton's iterative process in which the initial guess function is obtained through the parametric continuation method described in the text.

method, option 4, is considerable more expensive than collocation methods, options 2 and 3. Each one of these options practically require the same computing time.

In order to illustrate the efficiency of the parametric continuation scheme, in Fig. 3 we plot, with a continuous line, the value of the Euclidean norm before each iteration. The extrapolation scheme of Eq. (35) is used. The broken curve shows the same quantity when a previous solution is used as the initial estimate. From this figure it is clear that the number of iterations, and therefore the computational time, is reduced if parametric continuation is used.

## 5. SUMMARY

Determination of the reduced density profiles of planar electrical double layer for the primitive model of an electrolyte, according to the HNC/MSA theory, require the numerical solution of a system of nonlinear integral equations (one for each of the $n$ species present in the fluid). The successive-substitution method, traditionally employed in the solution of similar problems, is very expensive in terms of computational work. The finite element methods treated in this work are shown to be much more efficient. For example, if for a property like $\sigma$, an accuracy of less than two parts in $10^{-7}$ is required, option 1 with the mesh G6 results in a cost of more than 11 times the CPU time required by option 3 with the same mesh. Perhaps even more important is the fact that the number of iterations greatly increases for the successive substitution method when either concentration or the potential of the electrode is increased (4). In contrast, when coupled with Newton's method and the parametric continuation technique, the finite element procedures used here require only two to four iterations for steps in $\psi_0$ as large as 25 mV, with the convergence criterion $\Delta = 10^{-10}$.

The finite element approach used here is a modern numerical functional analysis [22]. For only a little additional effort, the technique can provide information on solution stability, sensitivity, and bifurcation analysis, which is unobtainable by traditional numerical methods.

From the results presented here, it is clear that the collocation criteria (option 3) combined with quadratic basis functions, has the virtue of being as accurate as the successive substitution method (option 1), and at the same time, is one of the two fastest options of this work. These characteristics make this option very atractive for applications similar to the problem solved here. In fact, it has been used for the determination of the temperature dependence of the double layer differential capacitance in the HNC/MSA approximation [23]. That study required extensive calculations that would be impracticable with traditional Picard iteration schemes.

The linear basis and the quadratic basis options in the collocation method use the same amount of computational time. However, the accuracy of the second one is much better than the first. Hence, it would be interesting to study the dependence of the efficiency and the accuracy of the collocation method with the degree of the polynomials used as basis functions. On the other hand, it is apparent from Table II

that for this problem, Galerkin's criteria does not represent an improvement in accuracy over the collocation criteria when linear basis functions are used. This is probably due to the use of the Swartz–Wendroff approximation. A study to clarify this question remains to be done.

## ACKNOWLEDGMENT

We gratefully acknowledge the support of CONACYT, México.

## REFERENCES

1. J. S. BARKER AND D. HENDERSON, *Rev. Mod. Phys.* **48**, 587 (1976).
2. R. O. WATTS, in Specialist Periodical Report, *Statistical Mechanics*, edited by K. Singer (Chemical Society, London, 1900), Vol. 1, p. 22.
3. J. M. ORTEGA AND W. C. RHEINBOLDT, *Iterative Solution of Nonlinear Equations in Several Variables* (Academic Press, New York, 1970) p. 181.
4. M. LOZADA-CASSOU, R. SAAVEDRA-BARRERA, AND D. HENDERSON, *J. Chem. Phys.* **77**, 5150 (1982).
5. M. LOZADA-CASSOU AND D. HENDERSON, *J. Phys. Chem.* **87**, 2821 (1983).
6. F. LADO, *J. Comput. Phys.* **8**, 417 (1971).
7. J. C. RASAIAH AND H. L. FRIEDMAN, *J. Chem. Phys.* **48**, 2742 (1968); **50**, 3965 (1969); J. C. RASAIAH, D. N. CARD, AND J. P. VALLEAU, *J. Chem. Phys.* **56**, 248 (1972); J. C. RASAIAH, *J. Chem. Phys.* **56**, 3071 (1972).
8. B. LARSEN, *J. Chem. Phys.* **68**, 4511 (1978).
9. L. MIER Y TERÁN, A. H. FALLS, L. E. SCRIVEN, AND H. T. DAVIS, in *Proceedings, 8th Symposium of Thermophysical Properties, National Bureau of Standards, Maryland*, 1981, edited by J. V. Sengers (ASME, New York, 1982), Vol. 1, p. 45.
10. S. E. QUIÑONES, B.Sc. thesis, Universidad de Guadalajara, México, 1983 (unpublished).
11. L. MIER Y TERÁN, E. FERNÁNDEZ-FASSNACHT, AND S. E. QUIÑONES, *Phys. Lett. A* **170**, 329 (1985).
12. L. MIER Y TERÁN AND E. FERNÁNDEZ-FASSNACHT, *Rev. Mex. Fis.* **32**, *S*241 (1986).
13. L. MIER Y TERÁN AND E. FERNÁNDEZ-FASSNACHT, *Phys. Lett. A* **117**, 43 (1986).
14. M. J. GILLAN, *Mol. Phys.* **38**, 1781 (1979).
15. G. ZERAH, *J. Comput. Phys.* **61**, 280 (1985).
16. D. HENDERSON, L. BLUM, AND M. LOZADA-CASSOU, *Progr. Surf. Sci.* **13**, 197 (1983).
17. JE. ALVAREZ, A. VALADEZ, AND JO. ALVAREZ, *Chem. Eng. Sci.*, in press.
18. G. STRANG AND G. J. FIX, *An Analysis of the Finite Element Method* (Prentice–Hall, Englewood Cliffs, NJ 1973) p. 116.
19. B. SWARTZ AND B. WENDROFF, *Math. Comput.* **23**, 37 (1969).
20. G. GOUY, *J. Phys.* **9**, 457 (1910).
21. D. L. CHAPMAN, *Philos. Mag.* **25**, 475 (1913).
22. W. W. SAWYER, *A First Look at Numerical Functional Analysis* (Claredon Press, Oxford, 1978).
23. L. MIER Y TERÁN, E. DÍAZ-HERRERA, M. LOZADA-CASSOU, AND D. HENDERSON, *J. Phys. Chem.* **92**, 6408 (1988).